Green Chemistry

PAPER

View Article Online
View Journal | View Issue

Cite this: *Green Chem.*, 2025, **27**, 14290

Polyesters incorporating biobased monomers for soil-release treatment of synthetic textile surfaces

Emanuella F. Fiandra, [a] Matthieu Starck, [a] Elliot K. Findlay,[a] Josephine Binks,[a] Gang Si,[b] Ruth Chilton,[b] Mark R. Sivik,[c] Richard L. Thompson, [a] Mark R. Wilson *[a] and Clare S. Mahon *[a]

Received 4th August 2025,
Accepted 14th October 2025

DOI: 10.1039/d5gc04056f

rsc.li/greenchem

Soil release polymers (SRPs) are used in laundry detergent formulations to enable the cleaning of textiles at lower wash temperatures and using shorter cycles. By modifying the fabric surface, SRPs prevent redeposition of soil during the wash cycle, and also assist with the removal of soil in the subsequent wash cycle. Most SRPs currently used in formulations contain petroleum-sourced building blocks, including terephthalic acid, potentially limiting the environmental benefit of their use. To improve the sustainability profile of these key additives, diglyoxylic acid xylose (DGAX, **1**), a monomer derived from hemicellulose, was used to partially replace the terephthalic acid component of SRPs. The ability of these copolymers to modify fabric surfaces was explored using anti-redeposition and soil release performance tests, in addition to contact angle and SEM analysis. The introduction of **1** within copolymers was found to further enhance the anti-redeposition performance on polyspandex fabrics, however, complete replacement of the terephthalic acid component with **1** resulted in polymers which displayed poor performance. These copolymer systems present a promising route to the development of high-performance and sustainable SRPs, particularly in offering performance across different synthetic textile surfaces.

Green foundation

1. Soil release polymers (SRPs) are used in laundry detergent formulations to enable effective cleaning performance during shorter cycles at low wash temperatures, presenting clear environmental benefits. Most SRPs are constructed using petroleum-derived building blocks, limiting their environmental benefits. Here, we report a new class of SRPs where a proportion of a petroleum-derived monomer, terephthalic acid, is replaced with a biomass-derived alternative, diglyoxylic acid xylose.
2. SRPs are shown to match the performance of conventional SRPs on polyester substrates and to exceed performance of currently used SRPs on polyspandex. These SRPs therefore present enhanced cleaning performance and an improved environmental profile.
3. Our studies have provided insights into the mechanism of surface modification by SRPs, which will guide the future design of biobased detergent additives.

Introduction

Synthetic polyester fibres were first introduced in the 1960s as a more durable and cheaper alternative to cotton and wool garments.[1] Synthetic fabrics can offer a more sustainable environmental footprint, as cotton is a highly water-intensive fabric during production and in fabric care and maintenance,[2] accounting for 69% of the water footprint for fibre production alone.[3,4] Polyester (typically poly(ethylene terephthalate), PET, Fig. 1) fabrics are low-cost, durable, easy-to-wash and wrinkle-free, with an annual production of 57 million tonnes in 2020, representing 52% of global fibre production.[5] Compared to cotton, synthetic fibres such as PET and polyspandex (PS, Fig. 1), a blend of PET and a polyurethane, are more regular in structure and hydrophobic in nature, which can lead to challenges in the removal of hydrophobic soil[6,7] such as grease, sebum, or cooking oil. The build-up of such soil on synthetic fabrics can lead to issues with the appearance[8] or odour[9,10] of fabrics, and loss of moisture comfort.[11] Within modern detergent formulations, polymer additives[12–17] are used to circumvent these challenges in soil-removal and to prevent transfer of dyes between fabrics, with improvements in cleaning performance sufficient to enable efficient cleaning under milder wash

[a]*Department of Chemistry, Durham University, Durham, DH1 3LE, UK. E-mail: clare.mahon@durham.ac.uk*
[b]*The Procter & Gamble Newcastle Innovation Centre, Whitley Rd, Newcastle upon Tyne, NE12 9BZ, UK*
[c]*Fabric & Home Care Innovation Center, The Procter & Gamble Company, Cincinnati, Ohio 45202, USA*

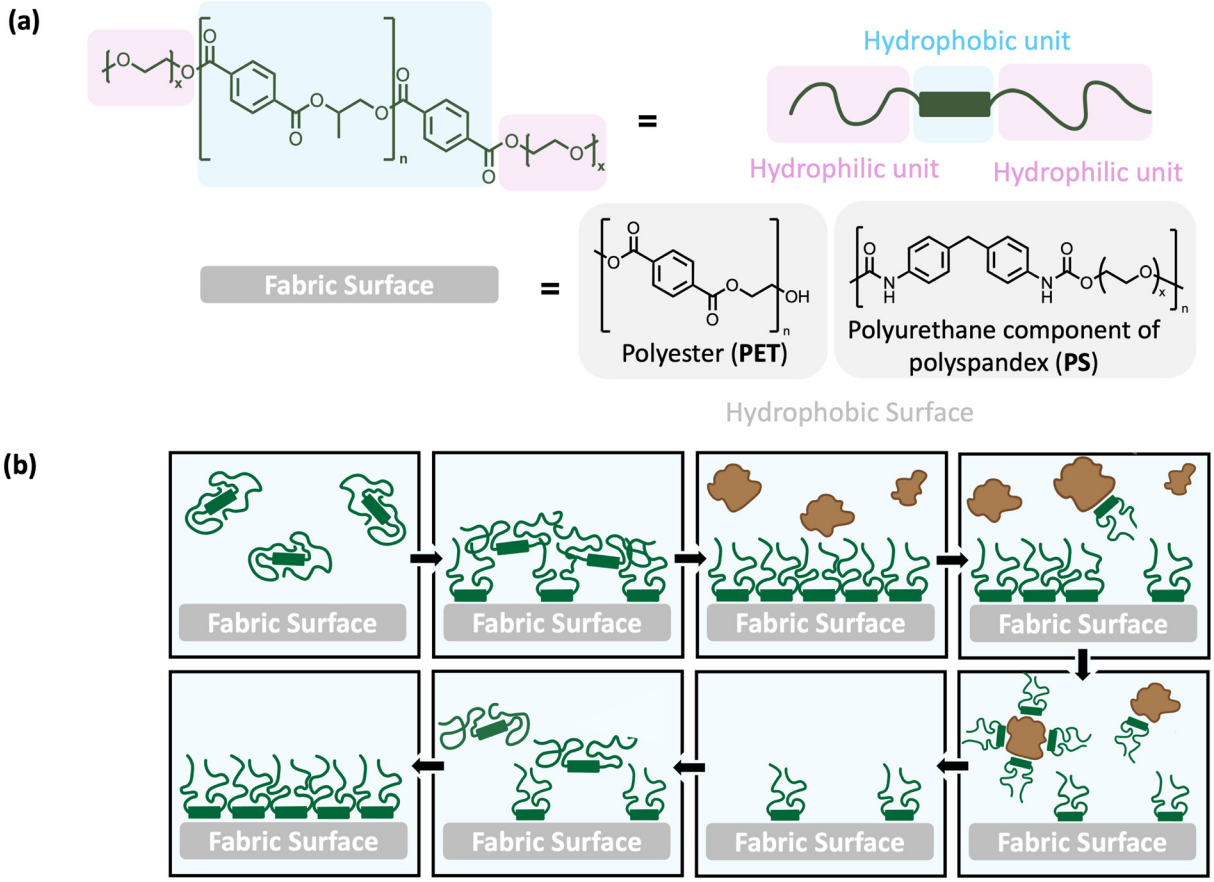

Fig. 1 (a) A conventional terephthalate-based SRP, with the hydrophilic and hydrophobic components highlighted and the hydrophobic fabric surfaces of interest: polyester (PET); and the polyurethane component of polyspandex (PS). (b) The proposed mechanism of SRP function. SRPs deposit on fabric surfaces, rendering the surface hydrophilic and hence preventing staining during the next wear phase, with multi-cycle enhancement during subsequent wash cycles.

settings of 30 °C, rather than 40 °C, facilitating energy reductions of up to 40% per cycle.[18]

Soil release polymers (SRPs) deposit on fibres, and hence change the surface properties,[19,20] delivering benefits such as reducing soil deposition onto the fabric during the wash cycle and further promoting the removal of soil from SRP-modified fabric surfaces in the next wash cycle (Fig. 1). SRPs also reduce the adhesion of allergens to the fabric,[21,22] reduce malodour on consumer garments,[23–27] and improve wicking properties.[28,29] These improvements in fabric appearance and comfort can also extend the service life of textiles, offering further sustainability benefits, with extended garment lifetimes contributing to reductions in the amounts of textile waste disposed of in landfill sites.[4] The presence of aromatic units in conventional SRPs is critical for their deposition, with these units predominantly derived from terephthalate monomers (Fig. 1a), which are obtained through the oxidation of petrochemically sourced *p*-xylene.[30] While advances have been made in the production of terephthalic acid from biomass,[31–33] these approaches are currently less efficient than traditional petrochemical routes. More generally, the need to move away from petrochemically-derived feedstocks has resulted in rising interest in sustainably sourced monomers[34] and monomers that are biobased,[35] to improve the sustainability profile of these key detergent additives.[36–39]

One attractive alternative to petrochemical-based feedstocks is the use of lignocellulosic biomass, due to the inherently degradable nature and high abundance of these materials.[40–43] Lignocellulose is comprised of three principal fractions: cellulose, hemicellulose and lignin; organised into macrofibrils which mediate the structural stability of plant cell walls.[44] Hemicellulose is the second most abundant component in lignocellulose, and when hydrolysed gives rise to the 5- and 6-carbon monosaccharides glucose, xylose, arabinose, galactose and mannose.[45] For low-cost production of sugars,[46] sources high in hemicellulose and low in lignin content such as birch wood[47] and corn cobbs[48] provide a promising supply. Manker *et al.* reported[49] the synthesis of biosourced polymers derived from monomers prepared from the hemicellulosic fraction extracted from birch wood in a high yielding, scalable process. In this approach, the fused heterotricyclic diacid diglyoxylic acid xylose (DGAX) (**1**), and the corresponding dimethyl ester, dimethylglyoxylate xylose, were produced though the reaction of xylose with diglyoxylic acid, and used to

make polyesters. It was additionally shown that these monomers can be accessed directly from hemicellulose *via* aldehyde-assisted fractionation[50] to produce xylose, which can then be transformed into the diacid monomers. Similar approaches have also been used to synthesise biobased surfactants from lignocellulosic biomass.[51–53] Lignocellulose and derivatives have been used[54] to permanently modify fabric surfaces to infer functionality such as UV resistance and fire retardancy, demonstrating the potential of these biomass derived materials to modify surface properties.

In this paper, we report the synthesis of a series of SRPs (**P1–P5**) that contain varying proportions of biobased monomer **1** and dimethyl terephthalate (**2**) and explore their performance in laundry detergent formulations. To gain further insight into the differences in wash performance and establish structure–property relationships, the behaviour of SRPs in solution and at the textile interface was studied in simplified systems using a range of techniques: contact angle measurements, scanning electron microscopy (SEM) and dynamic light scattering (DLS).

Molecular modelling was used to compare binding affinities for SRP cores to representative PET and PS surfaces, and provide insights into the folding and aggregation of SRPs in water. We demonstrate that incorporation of **1** into SRPs leads to strong binding to both fabrics, significantly increasing binding affinity for PS. However, strong intra-chain interactions between units of **1** increase solution aggregation such that SRPs containing larger proportions of **1** form larger aggregates (surrounded by a PEG corona) that do not adhere effectively to fabric surfaces. Combining **1** and **2** in the central block of the polymer disrupts solution aggregation, yielding SRPs that match the performance of currently used SRPs on PET, and show a markedly improved performance on PS fabrics.

Results and discussion

Polymer synthesis and characterisation

A series of poly(propylene terephthalate) (**P1**) and poly(propylene diglyoxylic acid xylose) (**P5**) based SRPs, and their corresponding copolymers (**P2–P4**) were prepared under classical melt polycondensation conditions (Scheme 1, Table 1), following a protocol adapted from the literature.[49] Classical melt polycondensation typically requires highly elevated temperatures due to the requirement for a bulk polycondensation to be at least 10 to 20 °C higher than the melting point of both monomers and polymers to achieve melt homogeneity.[55] Pentaerythritol tetrakis(3-(3,5-di-*tert*-butyl-4-hydroxyphenyl)propionate) (Irganox1010) was therefore added to reaction mixtures to avoid thermo-oxidative degradation of monomers.

Following this method, a series of homopolymers and copolymers were prepared using **1**/**2** as the dicarboxylate component (Table 1). The stoichiometric ratio of **1** and **2** was varied to produce polymers containing 0–100% **1** as the dicarboxylate component. The resultant polymers were analysed by ^{1}H NMR spectroscopy (SI section S8.2) and gel permeation chromatography (GPC) (SI section S2.5) to confirm the structure of the polymer, and determine the degree of polymerisation (DP) of each unit present in the hydrophobic block (Table 1). Consistent molecular weights of 5.2 to 6.0 kDa were attained across the series **P1–P5** (Table 1 and SI Fig. S1).

Anti-redeposition performance

The ability of **P1–P5** to function in laundry detergent formulations was initially investigated using anti-redeposition performance tests. Here, SRPs are evaluated for their ability to prevent the redeposition of suspended soil, transferred from a soiled fabric swatch, onto white fabric tracers during the wash process (Fig. 2a). The extent of soil redeposition is monitored

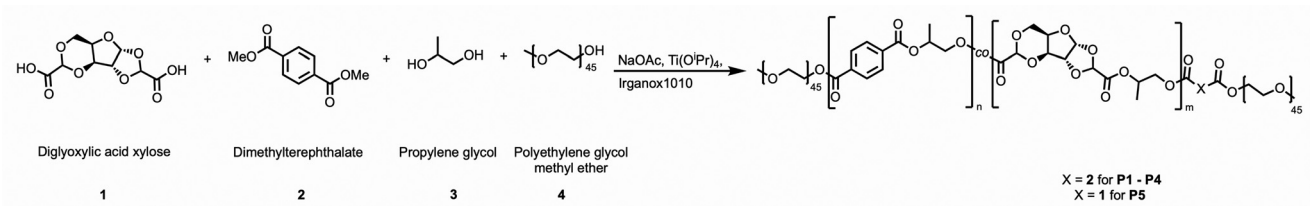

Scheme 1 Synthesis of SRPs **P1–P5** using a melt polycondensation approach.

Table 1 Synthesis and resultant structural parameters of SRPs. (eq.: molar equivalent)

Polymer	**1**/eq.	**2**/eq.	**3**/eq.	**4**/eq.	n^a	m^a	DP	% of **1**	M_n ^{a}/g mol^{-1}	M_n ^{b}/g mol^{-1}	M_w ^{b}/g mol^{-1}	$Đ^b$
P1	0	10	400	2	5	0	5	0	5200	5800	6400	1.1
P2	1	9	400	2	6	1	7	12	5600	6000	6600	1.1
P3	2	8	400	2	6	2	8	25	6000	6200	6800	1.1
P4	5	5	400	2	3	3	6	50	5600	5200	5900	1.1
P5	20	0	400	2	0	6	6	100	6000	5700	6200	1.1

^{a} As determined by ^{1}H NMR spectroscopy, using end-group –OCH_3 as reference for analysis. ^{b} As determined by gel permeation chromatography in 1.0 g L^{-1} LiBr in DMF at 50 °C (0.6 mL min^{-1}), calibrated against near monodisperse poly(methyl methacrylate) standards.

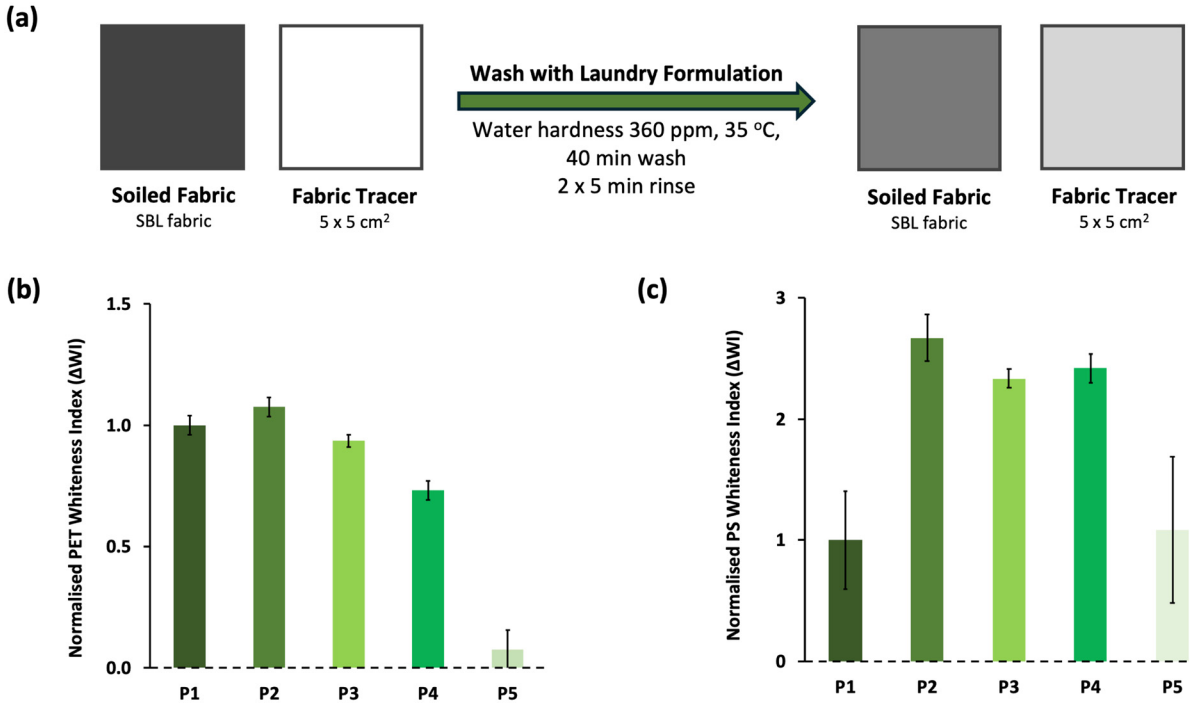

Fig. 2 (a) Anti-redeposition performance test under standard wash conditions; (b) normalised whiteness index (ΔWI) of polyester (PET) tracers and (c) normalised whiteness index (ΔWI) of polyspandex (PS) tracers washed with a laundry detergent formulated with 1% (w/w) SRP (**P1–P5**), with data normalised relative to **P5**. The baseline 0 indicates the performance of the polymeric additive-free negative control (Nil).

by assessing the whiteness index (WI) of the fabric tracers before and after washing under standard D65 illumination by image analysis (SI section S3.1).

A high-throughput tergotometer system was used to evaluate the anti-redeposition performance of **P1–P5**, with PET and PS tracers washed under representative wash conditions (40 min wash, 2 × 15 min rinse, 35 °C, water hardness 360 ppm, 4 cycles). Each wash load also included knitted cotton and polycotton fabric swatches to represent a consumer wash load, along with soil. Commercially-sourced artificial soil sheets (SBL2004 WFK, Krefeld, Germany) were cut into 5 × 5 cm^2 squares and included in each wash together with white PET and PS fabric tracers (also 5 × 5 cm^2 squares) with the soil consisting of vegetable oil, synthetic sebum and solid particles such as carbon black and kaolin.[13] Soiled fabric sheets were replaced after each wash cycle, and image analysis was used to quantify anti-redeposition performance in terms of the change in whiteness index (ΔWI) of PET or PS tracers. A negative control experiment (Nil) was performed, with no SRPs present in the detergent formulation, to allow for a direct comparison with detergent formulation containing SRPs under study (1% w/w). The ΔWI was determined by comparing the WI of fabric tracers washed with SRP-containing formulations to the WI of the negative control. SRPs that perform well produce a high positive ΔWI value.

P1, which is representative of conventional terephthalate-based SRPs, showed a significant whiteness benefit for PET fabrics (Fig. 2b), as expected due to its similarity in structure to the surface enabling favourable supramolecular interactions between the core block of the SRP and the PET surface.[56] Interestingly, copolymers **P2–P4** exhibited similar performance on PET, comparable to that of the homopolymer **P1**. Conversely, **P5** demonstrated little to no performance on PET fabric, demonstrating inclusion of a proportion of monomer **2** to be crucial to anti-redeposition performance. Results for **P2** and **P3**, however, suggest that equivalent anti-redeposition performance on PET fabrics can be achieved at dicarboxylate monomer compositions of up to 25% bioderived monomer **1**.

Interestingly, the anti-redeposition performance benefit of SRPs containing both dicarboxylate components (**P2–P4**) on PS fabric was greater than that of either **P1** or **P5**, with average ΔWI at least doubling in value (Fig. 2c). SRPs currently used in formulations typically display limited anti-redeposition performance on PS fabrics, analogous to observations for **P1**. PS fabrics are typically comprised of a blend of both PET and polyether–polyurea fibres, most commonly 95% PET and 5% polyether–polyurea. The inclusion of **1** therefore offers a marked benefit to SRP performance in extending anti-redeposition performance to PS fabrics, enabling effective cleaning of PS fabrics under environmentally favourable conditions.

Soil release performance

P1–P5 were subsequently evaluated in soil release performance tests to further investigate the surface modification capabilities of the SRPs. PET and PS tracers (5 × 5 cm^2) were preconditioned with a laundry detergent formulation containing 1%

w/w SRP in a high-throughput tergotometer system, mimicking typical consumer wash conditions (final SRP concentration 20 ppm, 40 min wash, 2 × 15 min rinse, 30 °C, water hardness 135 ppm, 3 cycles) (Fig. 3a). Each wash load included eight tracers and knitted cotton swatches to represent a consumer wash load. Once dried (50% relative humidity, 20 ± 2 °C), each fabric tracer was stained with 100 μL dirty motor oil (DMO) (SI, section S3.2) and left to dry overnight. Stained PET and PS tracers then underwent image analysis before washing under standard wash conditions (40 min wash, 2 × 15 min rinse, 30 °C, water hardness 135 ppm, 1 cycle), with the laundry detergent formulation used containing no SRPs. During the final wash stage, each load included two tracers of either PET or PS and knitted cotton garments. Four replicates were run in total for each polymer sample under investigation. Once dried, images were collected for each of the tracers, with the pre- and post-wash data analysed. Here, the colour of the fabric surface was characterised by measuring the L^* (lightness), a^* (redness), and b^* (blueness) coordinates, as defined by the CIELAB colour system.[57] The relative colour changes, ΔE^*, were then determined from the differences in these coordinates before and after the final wash cycle, which were then used to calculate the stain removal index (SRI) (SI, section S3.2).[13] Better-performing SRPs remove DMO from fabrics more effectively, represented by a higher SRI (%).

PET surfaces modified with **P2** resulted in an ΔSRI value of 66.2 ± 0.6% which was comparable to the conventional polymer **P1** (67.9 ± 0.1%) (Fig. 3b). This observation suggests that the incorporation of 12% of monomer **1** into the central block of the SRP does not negatively impact the soil release performance. **P3** and **P4**, however, displayed a significantly lower performance with ΔSRI values ranging from 20 to 29%. **P5** displayed the lowest ΔSRI value of 9 ± 2%, highlighting its inability to effectively facilitate the removal of DMO from a treated surface during a wash cycle. A different trend is observed when PS surfaces are treated with polymers containing **1** (Fig. 3c), with the copolymer **P3** displaying high ΔSRI value of 66 ± 1%, respectively, exceeding that of the conventional polymer **P1** (45 ± 1%). **P4** and **P5** displayed marked decreases in performance, however. In gravimetric sebum removal tests (SI section S3.3) **P2–P4** were observed to display comparable performance to the conventional SRP, **P1**, on PE and PS surfaces demonstrating that favourable serum release can be facilitated by SRPs containing a proportion of biomass-derived monomer **1**. However, the homopolymer **P5** showed no additional benefit compared to the negative control (Nil) highlighting the importance of the aromatic unit in enabling effective modification of PET and PS fabric surfaces.

Taken together, performance studies demonstrate that fabric surface modification has taken place, and show that comparable performance to SRPs currently used in formulations could be achieved on PET fabrics, while incorporating significant quantities of biobased monomer **1**. The soil-release and anti-redeposition performance of SRPs containing up to 50% **1** on PET surfaces were also comparable to those reported in our previous study[35] which employed biomass-derived pyri-

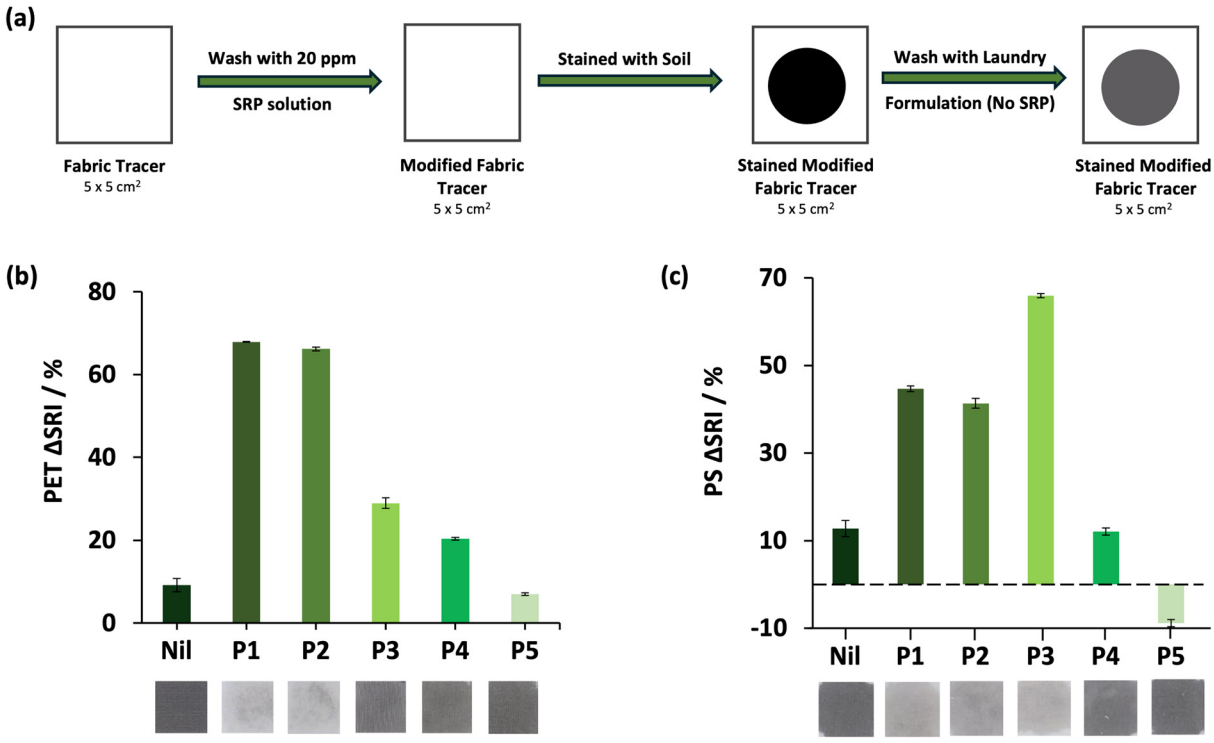

Fig. 3 (a) Soil release performance test conducted under standard wash conditions; (b) ΔSRI values obtained for the Nil and SRPs **P1** to **P5** on PET tracers; (c) ΔSRI values obtained for the Nil and SRPs **P1** to **P5** on PS tracers with photographs of the fabric tracers after performance testing.

dine dicarboxylate monomers. In the case of PS, however, the inclusion of monomer **1** improved the performance of SRPs beyond those currently in formulation, offering an enhanced overall environmental profile. The structural factors driving these differences in performance were not immediately evident, and we therefore conducted a series of experiments to investigate the solution behaviour and surface activity of SRPs using a simplified representative system.

Solution behaviour of SRPs

Solutions of **P1–P5** in water (1% w/w) were subjected to DLS analysis at 35 °C to investigate the species present in solution (Fig. 4). In each case, nanoscale aggregates were observed, with differences in the sizes of the aggregates evident from the correlation functions obtained (Fig. 4a).

In line with previous studies,[35] we identified a correlation between solution aggregation state and soil release performance. SRPs observed to self-assemble to yield larger aggregates (*e.g.* **P5** D_h 100 nm at 1% w/w), were found to display poor performance, while polymers observed to form smaller aggregates (*e.g.* **P1–P3** D_h 10–20 nm) were shown to function more effectively.

To understand the factors that contribute to the observed aggregation of **1**-containing SRPs, umbrella sampling simulations were performed on the association of two molecules of **P4**, and two molecules of **P5**, to obtain a potential of mean force (PMF), where the reaction coordinate is the separation between the centre of mass of each core unit (Fig. 5a). An aggregate of two polymers was equilibrated in solution using a general molecular dynamics workflow, before steered molecular dynamics (SMD)[58] was applied to separate the polymers at a rate of 1 Å ns^{-1}, from the minimum possible distance to a maximum of 99 Å. Snapshots from the SMD simulations were captured at distances from the minimum to 99 Å, with a separation of roughly 1 Å between windows. Each window simulation was then run for 40 ns, with a restraint potential of 2.5 kcal mol^{-1} to keep the polymers in place. The configurations from these simulations were then reweighted using the weighted histogram analysis method (WHAM)[59] and combined to generate the PMF for each SRP aggregate complex.

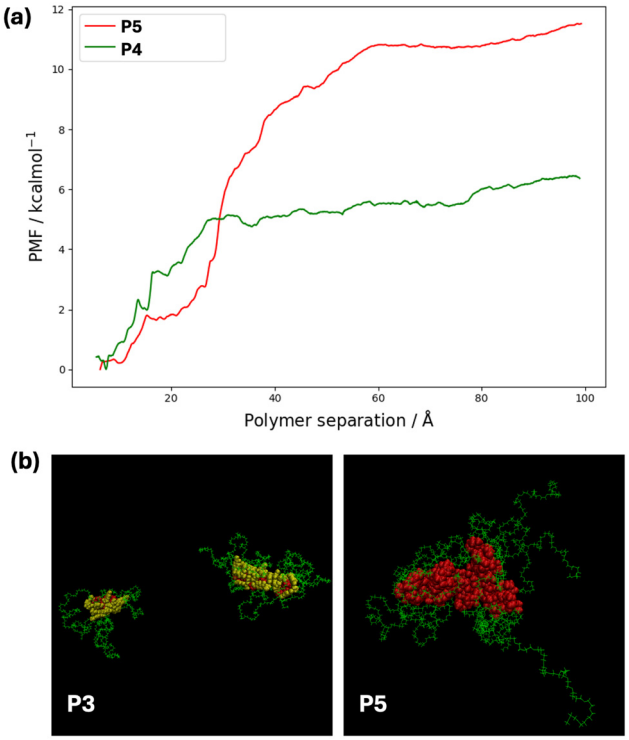

Fig. 5 (a) Potential of mean force (PMF) obtained from umbrella sampling calculations for the cores of **P5** and **P4** as a function of separation between the centres of the polymer chains. (b) Representative snapshots of **P3** and **P5** at 1% (w/w) solution after 15 ns of simulation time. PEG chains are represented as lines in green, monomer **1** is shown as van der Waals radii in red and monomer **2** is shown as van der Waals radii in yellow.

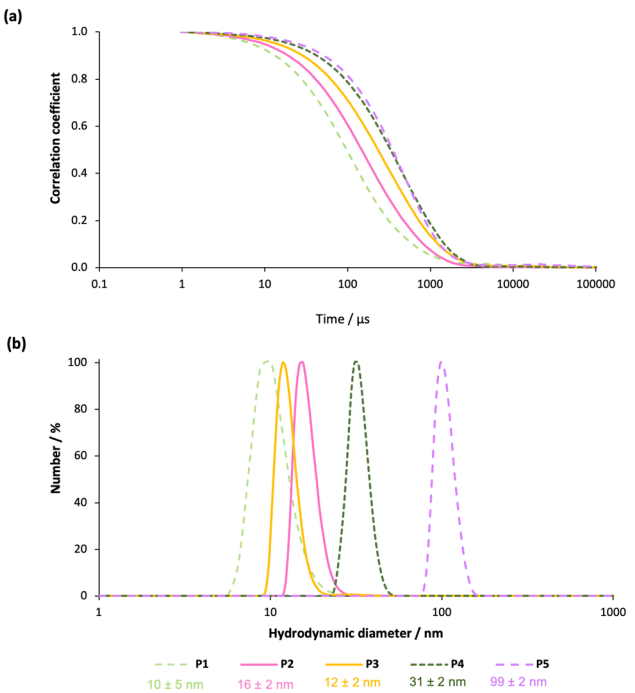

Fig. 4 (a) DLS correlation functions. (b) Normalised number average particle size distributions, with indicative average D_h for SRP in an aqueous solution (1.0% w/w), with measurements recorded at 35 °C.

The difference in free energy of aggregation can then be derived from the PMF plot by subtracting the energy of the plateau region (full separation) from the energy of the bound state (minimum distance), which is normalised to 0 kcal mol^{-1}.

Simulations suggest that the aggregation of **P5** is energetically more favourable than that of **P4**, with significantly more energy required to separate the cores (Fig. 5a). It is likely that this aggregation is driven by strong hydrophobic effects. Affinity between units of **2** is also evidenced in simulations where five **P3** and **P5** polymer molecules were studied in 1% (w/w) solution (Fig. 5b, SI section S7.4). Larger aggregates are present after 20 ns for **P5** compared to **P3**, consistent with the observation of larger assemblies in DLS studies. For **P3**, inter-core interactions are mainly mediated by π–π stacking but this

is disrupted by the presence of **1**. Moreover, π–π stacking in water is sufficiently weak to be dynamic[60,61] allowing relatively rapid chain refolding, as seen in our previous work on pyridine dicarboxylate-based polymers.[35]

Surface activity of SRPs

A primary function of SRPs is the hydrophilisation of hydrophobic surfaces, proposed to occur through the binding of the hydrophobic block of the polymer to the surface of the fabric, resulting in the hydrophilic blocks being positioned at the aqueous interface through molecular orientation (Fig. 1). To investigate the ability of the SRPs to modify fabric surfaces, solutions of **P1–P5** were deposited on model surfaces representing the chemical composition of PE and PS fabrics. Model PET surfaces were created by spin-coating a solution of amorphous PET (amPET, 1% w/w in $CHCl_4$) onto silicon wafer (1500 rpm, 30 s). A similar method was followed to create a surface which approximates the composition of PS, using a blend of amPET and polyurethane (95 : 5) solution (1% w/w in THF) spin-coated onto a silicon wafer (2000 rpm, 30 s). The model PET and PS surfaces were shown to display average water contact angles of 70.1° and 63.3°, respectively, indicative of hydrophobic surfaces.

Surfaces were then treated with a solution of SRP (**P1–P5**, 1% w/w) for 40 min, then inverted to allow for the removal of undeposited SRP. A 5 μL droplet of deionised water was then placed on each of the SRP-treated surfaces, with the contact angle measured at room temperature (SI Fig. S4). All surfaces modified with SRP displayed a reduction in the contact angle, ranging from 5.0° to 19.4° (SI Fig. S4), suggesting deposition of polymer and surface hydrophilisation.

Water contact angles were measured after the SRP-modified surfaces underwent a dip rinse (Fig. 6), to better reflect the overall wash process and provide a greater understanding regarding the extent of surface deposition. On PET surfaces treated with **P2–P4**, contact angles between 10.1 and 21.3° were observed, in line with the contact angle observed for surfaces treated with **P1** (19.2°), suggesting that surface hydrophilization has been retained. The PET surface treated with **P5** displayed an increased contact angle after rinsing (39.6°), suggesting a decrease in effective SRP surface concentration and increased hydrophobicity, which may account for the poor soil-release performance observed. PS surfaces treated with **P2** and **P3** displayed contact angles after rinsing of 18.3 to 20.5°, in line with that displayed by a surface treated with **P1** and rinsed (21.5°). Surfaces treated with **P4** and **P5** displayed an increased contact angle after rinsing (41.1–44.7°). This relative surface hydrophobicity is consistent with the poor performance of these polymers in soil-release tests (Fig. 3), suggesting that these SRPs are easily removed from the surface by rinsing.

SEM imaging was performed to gain further insight into the deposition of the SRPs on both PET and PS fabric surfaces. Samples for SEM analysis were prepared by soaking 1 × 1 cm^2 fabric swatches in solutions of **P1–P5** (1% w/w) (210 rpm, 35 °C). Fabrics were air dried overnight before sputter coating with a gold–palladium conducting layer. SEM images were

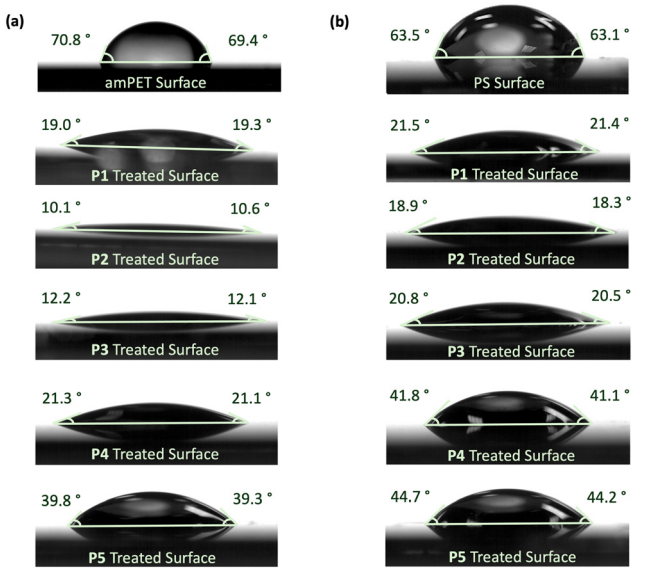

Fig. 6 Contact angle measurements of a 5 μL droplet of deionised water on a (a) amPET surface and 1% (w/w) SRP-treated amPET surface; (b) PS surface and 1% (w/w) SRP-treated PS surface; after dip rinsing in H_2O.

then taken at a range of magnifications (Fig. 7 and SI Fig. S5, S6) to show the morphological changes to fabric fibres as SRP deposit and modify their surface. A reference sample was imaged to allow for a direct comparison between an unmodified and modified fabric surface. In each case, changes in surface morphology were evident, consistent with deposition of SRPs **P1–P5** on surfaces.

Image analysis of the reference PET sample (Fig. 7a and SI Fig. S5) showed the presence of a textured surface with sharp elements raised on the surface with a maximum length of 2 μm. Despite these sharp elements remaining present to some extent after SRP-surface modification, surfaces treated with **P1–P4** appear smoother, suggesting that SRPs have coated the surface of the fibres. The presence of SRPs was also highlighted by the build-up of polymer in the gaps of the fibres, thereby increasing the surface area and eliminating potential locations for soil to collect (Fig. 7a, feature 1). Surfaces treated with poorly-performing **P5** appeared to be more textured, with additional build-up on the surface as the raised elements increased in size to greater than 2 μm and were more irregular in topology compared to the reference fabric. This irregularity in surface topology may partially account for the increased deposition of hydrophobic material on these surfaces.

Images were also collected for PS textiles (Fig. 7b and SI Fig. S6). Here, the reference PS showed a highly irregular structure that was very textured with crystalline features. The fabric treated with **P1** displayed a similar appearance to the reference fabric, which could contribute to the poor performance of this SRP. Incubation in solutions of **P1–P3** appeared to smooth the surface to varying extents, with notable improvements in morphology noted for **P2**. Surfaces treated with **P4** and **P5** displayed similar surface morphologies to unmodified PS, includ-

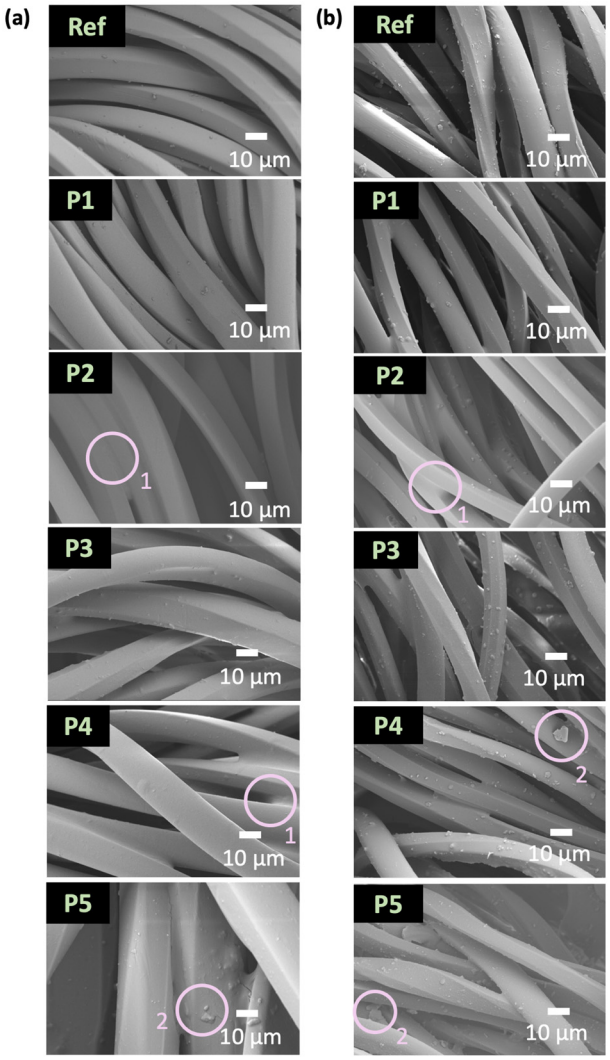

Fig. 7 SEM images taken at a magnification of 1000× for (a) PET and the PET-SRP modified fabrics (**P1** to **P5**) with a gold–palladium sputter coating thickness of around 33 nm; (b) PS and the PS-SRP modified fabrics (**P1** to **P5**) with a gold–palladium sputter coating thickness of around 49 nm. Some features have been highlighted: (1) SRPs appearing to deposit between fibres; (2) irregular deposits on fibres.

ing the presence of irregular deposits (Fig. 7b, feature 2), which may suggest a higher degree of heterogeneity in surface modification with SRP.

To rationalise the differences in interfacial behaviour observed, we calculated surface binding energies for truncated SRP core units and model PET and PS surfaces using a MM/PBSA[62] approach (Table 2; SI section S7.3). The calculated modified free energy of binding $\Delta G'_{bind}$ represents a combination of energy gained through non-covalent surface association, including van der Waals and electrostatic interactions, solvation effects, and also incorporates the contribution of chain folding in aqueous solution. Notably, the calculated binding energies correlate with the observed performance in anti-redeposition studies (Fig. 2b and c). Core structures containing **2**, or combinations of **1** and **2**, were predicted to interact favourably with both PET and PS surfaces. The addition of **1** to the core was observed to increase affinity to the surfaces (ΔG_{bind}). The overall strongest binding, $\Delta G'_{bind}$, predicted for **P3** cores on a PET surface. Calculated $\Delta G'_{bind}$ values for association of copolymer cores **P2–P4** with PS surfaces are more favourable than that of **P1**, explaining their enhanced performance on this substrate. The inclusion of **1** in the core, however, was predicted to increase the favourability of self-association (ΔG_{fold}), in line with PMF calculations demonstrating strong self-interactions (Fig. 5a) and the observation of large aggregates in DLS studies (Fig. 4b). The surfaces of these large aggregates are likely to be highly hydrophilic as a consequence of the high density of PEG chains within the corona, and they are therefore either unlikely to deposit on a hydrophobic fabric surface, or are likely to be easily removed by rinsing. Interestingly, calculations suggested that **P5**, which contained **1** as the sole dicarboxylate component and displayed poor performance, would interact favourably with PET and PS surfaces (ΔG_{bind}). Effective performance is likely prevented by the tendency of **P5** to form large aggregates in solution (Fig. 4b), driven by significant self-association (ΔG_{fold}). The inclusion of **2** suppresses aggregation in solution (Fig. 4b), with reductions in calculated ΔG_{fold} observed. These observations may suggest that an important role of the terephthalate component in enabling SRP performance within this series is in suppression of aggregation, in addition to directly interacting with the fabric surface, presenting opportunities to replace **2** with another biobased monomer, to further improve the sustainability profile of the SRPs.

Conclusions

The incorporation of a proportion of biosourced monomer **1** in SRPs yielded promising performance benefits, matching those of conventional SRP **P1** on PET substrates, and exceeding the performance of **P1** on PS substrates. While all polymers were demonstrated to modify and hydrophilise representative surfaces through contact angle and SEM studies, we have identified a correlation between solution aggregation and performance which affords molecular-level insight into the mechanism of effective surface modification, and explains differences in performance observed. Polymers which formed smaller aggregates, as assessed through DLS studies, were observed to display enhanced performance in anti-redeposition and soil-release tests compared to those which form larger aggregates. Molecular modelling studies predict this self-association behaviour, and suggest that aggregation is driven by strong hydrophobic effects. Binding energies have been calculated for SRPs on model fabric surfaces, calculated using a MM/PBSA method which incorporates surface interaction, solvation and folding effects. These calculations support the differences in performance observed, with polymers predicted to engage in thermodynamically favourable interactions with model surface observed to perform well, while the interaction of polymer **P5**, which displayed no favour-

Table 2 Energies obtained from MM/PBSA calculations for each truncated polymer core on model PET and PS surfaces. The full details of the binding calculations are given in the SI (section S7.3), where $\Delta G_{gas} = \Delta G_{complex} - \Delta G_{surface} - \Delta G_{molecule}$ is the binding energy in the absence of any solvent; ΔG_{solv} is the PBSA solvent corrections to ΔG_{gas}; $\Delta G_{bind} = \Delta G_{gas} + \Delta G_{solvent}$; ΔG_{fold} is the folding free energy in implicit solvent; and $\Delta G'_{bind} = \Delta G_{bind} - \Delta G_{fold}$

Polymer core	Surface	ΔG_{gas}/kcal mol^{-1}	ΔG_{solv}/kcal mol^{-1}	ΔG_{bind}/kcal mol^{-1}	ΔG_{fold}/kcal mol^{-1}	$\Delta G'_{bind}$/kcal mol^{-1}
P1	PET	−101.63 (0.63)	85.45 (0.40)	−16.18 (0.66)	−9.00 (0.31)	−7.18 (0.73)
P2	PET	−114.98 (0.78)	94.84 (0.51)	−20.14 (0.85)	−10.97 (0.37)	−9.17 (0.93)
P3	PET	−120.79 (0.84)	99.28 (0.54)	−21.52 (0.89)	−9.37 (0.41)	−12.14 (0.98)
P4	PET	−109.98 (0.77)	89.38 (0.46)	−20.60 (0.79)	−13.51 (0.40)	−7.08 (0.88)
P5	PET	−127.40 (0.87)	100.69 (0.50)	−26.71 (0.90)	−29.29 (0.45)	2.57 (1.01)
P1	PS	−95.16 (0.61)	82.33 (0.40)	−12.83 (0.65)	−8.40 (0.30)	−4.43 (0.72)
P2	PS	107.54 (0.77)	90.85 (0.50)	−16.69 (0.84)	−10.44 (0.37)	−6.26 (0.92)
P3	PS	−115.08 (0.83)	96.32 (0.53)	−18.76 (0.89)	−8.97 (0.41)	−9.79 (0.98)
P4	PS	−105.72 (0.75)	87.53 (0.45)	−18.19 (0.77)	−12.80 (0.39)	−5.39 (0.86)
P5	PS	−122.39 (0.88)	97.89 (0.50)	−24.49 (0.91)	−27.78 (0.45)	3.28 (1.01)

able performance, was predicted to be thermodynamically unfavourable on both PET and PS surfaces. Effective surface modification likely requires binding of individual polymer entities to surfaces, in order for the hydrophobic core to interact with the fabric surface. SRPs that display solution aggregation are likely to display either limited deposition on surfaces, on account of shielding of the hydrophobic core by PEG blocks, or to be readily removed by rinsing.

SRPs containing **1** offer an improved sustainability profile to those currently used in formulation, as their performance extends to PS fabrics, offering the benefits of improved cleaning performance at low wash temperatures to an important class of textiles. A limitation of the SRPs described here is the requirement for the incorporation of terephthalic acid within the central block of the polymer. Developments in the production of biosourced terephthalic acid[31–33] may offer a route to SRPs with an enhanced sustainability profile. Alternatively, it is possible that other biosourced monomers, such as the pyridine dicarboxylates used in our previous study,[35] or other hemicellulose-derived diacids, could be used to replace the terephthalate component altogether. Furthermore, building on the work of Manker *et al.*,[49] the possibility of preparing polymers directly from hemicellulosic biomass could be explored. SRPs constructed using modified polysaccharides have been demonstrated[13] to display favourable soil-release performance on PET surfaces, highlighting further opportunities in the development of biosourced alternative additives.

In addition to presenting detergent additives of enhanced performance and improved sustainability profile, our studies have additionally enhanced understanding of the mechanism of action of SRPs. This mechanistic understanding will guide in the future design of biosourced SRPs, with a view to improving the environmental footprint of these key additives.

Author contributions

E. F. F.: investigation, methodology, data curation, writing – initial draft; M. S.: investigation, methodology, data curation; E. K. F.: investigation, methodology, data curation; J. B.: investigation, methodology, data curation; G. S.: conceptualisation, resources, supervision, writing – review and editing R. C.: investigation, methodology, data curation; M. R. S.: resources, writing – review and editing; R. L. T.: resources, supervision, M. R. W.: funding acquisition, investigation, supervision, writing – review and editing; C. S. M.: conceptualisation, funding acquisition, resources, supervision, writing – review and editing.

Conflicts of interest

There are no conflicts to declare.

Data availability

Data supporting this article has been included within the supplementary information (SI). Supplementary information: synthetic and experimental methods, characterisation, additional performance testing data, calculations. See DOI: https://doi.org/10.1039/d5gc04056f.

Acknowledgements

This work was supported by the Engineering and Physical Sciences Research Council [UKRI Future Leaders Fellowship MR/V027018/1; ANTENNA Prosperity Partnership EP/V056891/1; SOFI2 CDT EP/S023631/1]. The authors tahnk Dr Juan A. Aguilar of teh NMR service, and Peter Stokes of the mass spectrometry service at Durham University, for assistance with experiments.

References

1 F. Rodriquez, C. Cohen, C. K. Ober and L. A. Archer, *Principles of Polymer Systems*, CRC Press, Boca Raton Florida, 6th edn, 2015.
2 Z. Zhang, J. Huang, Y. Yao, G. Peters, B. Macdonald, A. D. La Rosa, Z. Wang and L. Scherer, *Nat. Rev. Earth Environ.*, 2023, **4**, 703–715.

3 *Fixing fashion: clothing consumption and sustainability*, Environmental Audit Committee, House of Commons, 2019.
4 *Valuing our clothes: The cost of UK fashion*, WRAP, 2017.
5 S. Opperskalski, S. J. Ridler, S. Y. Siew, E. Tan, L. Barsley, H. Denes, A. Gillespie, A. Gosai, A. Heaton, T. Hyde, N. Lambert, S. Marquardt, S. Seisl, L. Truscott, C. Weldon and P. Bettany, *Preferred Fiber & Materials Market Report*, Textile Exchange, 2021.
6 S. Chen, S. Zhang, M. Galluzzi, F. Li, X. Zhang, X. Yang, X. Liu, X. Cai, X. Zhu, B. Du, J. Li and P. Huang, *Chem. Eng. J.*, 2019, **358**, 634–642.
7 Y.-S. Chi and S. K. Obendorf, *J. Surfactants Deterg.*, 1999, **2**, 1–11.
8 T. Cooper and S. Claxton, *J. Cleaner Prod.*, 2022, **351**, 131394.
9 F. V. Herreweghen, C. Amberg, R. Marques and C. Callewaert, *Microorganisms*, 2020, **8**, 1709.
10 M. M. Abdul-Bari, R. H. McQueen, A. P. de la Mata, J. C. Batchellet and J. J. Harynuk, *Text. Res. J.*, 2020, **90**, 2212–2222.
11 C. W. Kan and C. W. M. Yuen, *Nucl. Instrum. Methods Phys. Res., Sect. B*, 2008, **266**, 127–132.
12 F. W. Marco and P. G. Harris, *EP. Pat*, EP0023361B1, 1983.
13 M. D'Avino, R. Chilton, G. Si, M. R. Sivik and D. A. Fulton, *Ind. Eng. Chem. Res.*, 2022, **61**, 14159–14172.
14 R. P. Rudy and A. A. Romano, *US Pat*, US 6426379B1, 2002.
15 S. J. Boardman, A. S. Hayward, N. J. Lant, R. D. Fossum and P. D. Thornton, *J. Appl. Polym. Sci.*, 2021, **138**, 49632.
16 V. N. G. Kumar and A. Moulee, *US. Pat*, US 6764992B2, 2004.
17 R. Rathinamoorthya, N. Ayswarriya, R. Kadambari, R. Sreelatha and K. G. Janani, *Indian J. Fibre Text. Res.*, 2016, **41**, 432–439.
18 *Save Energy in Your Home*, Energy Saving Trust 2017.
19 S. Pavlidou and R. Paul, *3 - Moisture management and soil release finishes for textiles*, Woodhead, Woodhead Publishing Series in Textiles, 2015.
20 A. Valentini, S. Bakalis, K. Gkatzionis, G. Palazzo, N. Cioffi, C. Di Franco, E. Robles, A. Brooker and M. M. Britton, *Ind. Eng. Chem. Res.*, 2019, **58**, 14839–14847.
21 P. Barreleiro, M. Weide, M. Hutmacher, R. Simmering and N. Wrubbel, *WO. Pat*, WO2014079755, 2015.
22 P.-P. Vinuesa, E. Maria and M. Jennewein, *EP. Pat*, EP2135931, 2009.
23 M. Peeters, A. Jacques and D. More, *WO. Pat*, WO2007059532, 2006.
24 M. Carvell, S. Dixon, K. Metcalfe and J. W. H. Yorke, *EP Pat*, EP3650522, 2018.
25 G. Si, M. McDonnell, M. Gillissen and H. Yamada, *WO. Pat*, WO2021118814, 2021.
26 M. Gillissen, H. Yamada, G. Si and M. McDonnell, *WO. Pat*, WO2021116049, 2019.
27 K. L. M. Depoot and J. A. A. Maes, *EP. Pat*, EP3587546, 2018.
28 R. Langevin, R. Panandiker and B. Loughnane, *WO. Pat*, WO2020005879A1, 2018.
29 A. Guttentag, *WO. Pat*, WO2022072399, 2022.
30 R. A. F. Tomás, J. C. M. Bordado and J. F. P. Gomes, *Chem. Rev.*, 2013, **113**, 7421–7469.
31 M. Volanti, D. Cespi, F. Passarini, E. Neri, F. Cavani, P. Mizsey and D. Fozer, *Green Chem.*, 2019, **21**, 885–896.
32 Y. Tachibana, S. Kimura and K.-i. Kasuya, *Sci. Rep.*, 2015, **5**, 8249.
33 J. Louw, S. Farzad and J. F. Görgens, *Biochem. Eng. J.*, 2024, **210**, 109404.
34 *UKBioChem10: The Ten Green Chemicals which can Create Growth, Jobs and Trade for the UK*, The Lignocellulosic Biorefinery Network, 2019.
35 M. Starck, E. F. Fiandra, J. Binks, G. Si, R. Chilton, M. Sivik, R. L. Thompson, J. Li, M. R. Wilson and C. S. Mahon, *JACS Au*, 2025, **5**, 666–674.
36 E. F. Fiandra, L. Shaw, M. Starck, C. J. McGurk and C. S. Mahon, *Chem. Soc. Rev.*, 2023, **52**, 8085–8105.
37 A. F. Sousa, C. Vilela, A. C. Fonseca, M. Matos, C. S. R. Freire, G. J. M. Gruter, J. F. J. Coelho and A. J. D. Silvestre, *Polym. Chem.*, 2015, **6**, 5961–5983.
38 I. Delidovich, P. J. C. Hausoul, L. Deng, R. Pfützenreuter, M. Rose and R. Palkovits, *Chem. Rev.*, 2016, **116**, 1540–1599.
39 A. Pellis, J. W. Comerford, S. Weinberger, G. M. Guebitz, J. H. Clark and T. J. Farmer, *Nat. Commun.*, 2019, **10**, 1762.
40 R. M. O'Dea, J. A. Willie and T. H. Epps III, *ACS Macro Lett.*, 2020, **9**, 476–493.
41 F. H. Isikgor and C. R. Becer, *Polym. Chem.*, 2015, **6**, 4497–4559.
42 G. W. Huber, S. Iborra and A. Corma, *Chem. Rev.*, 2006, **106**, 4044–4098.
43 W. Deng, Y. Feng, J. Fu, H. Guo, Y. Guo, B. Han, Z. Jiang, L. Kong, C. Li, H. Liu, P. T. T. Nguyen, P. Ren, F. Wang, S. Wang, Y. Wang, Y. Wang, S. S. Wong, K. Yan, N. Yan, X. Yang, Y. Zhang, Z. Zhang, X. Zeng and H. Zhou, *Green Energy Environ.*, 2023, **8**, 10–114.
44 A. A. Houfani, N. Anders, A. C. Spiess, P. Baldrian and S. Benallaoua, *Biomass Bioenergy*, 2020, **134**, 105481.
45 H. V. Scheller and P. Ulvskov, *Annu. Rev. Plant Biol.*, 2010, **61**, 263–289.
46 L.-Z. Huang, M.-G. Ma, X.-X. Ji, S.-E. Choi and C. Si, *Front. Bioeng. Biotechnol.*, 2021, **9**, 690773.
47 K. Gabov, R. J. A. Gosselink, A. I. Smeds and P. Fardim, *J. Agric. Food Chem.*, 2014, **62**, 10759–10767.
48 P. K. Gandam, M. L. Chinta, N. P. P. Pabbathi, A. Velidandi, M. Sharma, R. C. Kuhad, M. Tabatabaei, M. Aghbashlo, R. R. Baadhe and V. K. Gupta, *J. Energy Inst.*, 2022, **101**, 290–308.
49 L. P. Manker, G. R. Dick, A. Demongeot, M. A. Hedou, C. Rayroud, T. Rambert, M. J. Jones, I. Sulaeva, M. Vieli, Y. Leterrier, A. Potthast, F. Maréchal, V. Michaud, H.-A. Klok and J. S. Luterbacher, *Nat. Chem.*, 2022, **14**, 976–984.

50 S. Zheng, S. Sun, L. P. Manker and J. S. Luterbacher, *Acc. Chem. Res.*, 2025, **58**, 877–892.
51 S. Bertella, A. Komarova, S. Sun and J. Luterbacher, *EP. Pat*, EP4311826, 2022.
52 A. Komarova, S. Sun, S. Bertella and J. Luterbacher, *WO. Pat*, WO2023198682, 2023.
53 S. Bertella, A. Komarova, S. Sun and J. Luterbacher, *EP. Pat*, EP4311831, 2022.
54 J. Ruwoldt, F. H. Blindheim and G. Chinga-Carrasco, *RSC Adv.*, 2023, **13**, 12529–12553.
55 K. Matyjaszewski and M. Möller, *Polymer Science: A Comprehensive Reference Volume 5: Polycondensation*, Elsevier, 2013.
56 A. Ketema and A. Worku, *J. Chem.*, 2020, **2020**, 6628404.
57 Colorimetry, *ISO/CIE 11664-4:2019(E)*, 1976.
58 H. Grubmüller, B. Heymann and P. Tavan, *Science*, 1996, **271**, 997–999.
59 S. Kumar, J. M. Rosenberg, D. Bouzida, R. H. Swendsen and P. A. Kollman, *J. Comput. Chem.*, 1992, **13**, 1011–1021.
60 F. Chami and M. R. Wilson, *J. Am. Chem. Soc.*, 2010, **132**, 7794–7802.
61 G. Yu, M. Walker and M. R. Wilson, *Phys. Chem. Chem. Phys.*, 2021, **23**, 6408–6421.
62 E. Wang, H. Sun, J. Wang, Z. Wang, H. Liu, J. Z. H. Zhang and T. Hou, *Chem. Rev.*, 2019, **119**, 9478–9508.